ADVANCED FUNCTIONAL MATERIALS
www.afm-journal.de

Electrically Tunable Chiral Ferroelectric Nematic Liquid Crystal Reflectors

*Md Sakhawat Hossain Himel, Kelum Perera, Alex Adaka, Parikshit Guragain, Robert J. Twieg, S. Sprunt, James T. Gleeson, and Antal Jákli**

Manipulating light is an important area of optical research and development. To that end, tunable dichroic devices in which the reflectivity at differing wavelengths can be adjusted, are particularly valuable. This work is motivated by recent studies of the optical properties of chiral ferroelectric nematic liquid crystals (FNLCs). Here electro-optical studies are presented on two room temperature, FNLC materials that demonstrate electrically tunable reflectivity when subject to a field below 0.2 V μm^{-1}. Moreover, under appropriate conditions, the reflectivity can also be electrically (and reversibly) tuned (without change of color) from 0% to 40%. Reversible, low voltage tunable mirrors, having miniscule power consumption and operable around ambient temperature are expected to be useful in diverse applications ranging from energy-saving, smart windows to virtual reality interfaces.

1. Introduction

Controlling transmission and reflection of light is one of the most important branches of current research with potential applications as diverse as energy-saving smart windows[1,2] to augmented reality display devices.[3] One of the best-known materials capable of selective reflection of light is chiral nematic (also known as cholesteric) liquid crystals.[4] Cholesteric liquid crystals (CLCs) can form when elongated molecules capable of forming a nematic LC phase are doped with chiral additives. In the CLC phase, the center of masses of the molecules are randomly distributed in space. However, these materials are optically anisotropic, and the direction of their optical axis, a unit vector called the director, ($\hat{n}$), follows a helix. The helical pitch, p, is typically inversely proportional to the concentration of the chiral dopant. With the correct pitch, the material can exhibit a photonic bandgap, $\Delta\lambda = (n_e - n_o)p$ in the visible range, which is centered at a wavelength $\lambda = \bar{n} \cdot p$. n_e, n_o and $\bar{n}$ are the extraordinary, ordinary and average refractive indices, respectively. Since p typically depends on temperature, CLCs can be used as temperature sensors.[5,6] The helical structure is also sensitive to external electric and magnetic fields. In particular, the pitch normally increases with the field having a direction perpendicular to the helical axis, as predicted.[4,7] If either the electric field or the magnetic field is strong enough, the helix can unwind completely, resulting in a uniform optical axis configuration. These phenomena were demonstrated experimentally by Meyer in magnetic fields[7] and Kahn in electric fields.[8] However, when the CLC is confined between surfaces that have been treated to promote the director alignment, the surface interaction is usually sufficiently strong that the external field necessary to unwind the helix is not practically achievable. In this case, even though the structure becomes deformed from a perfect helix, the pitch remains unchanged. For electric fields, this typically occurs for fields above 1 V μm^{-1}.[9–12]

Significant improvements in low electric field tuning of chiral liquid crystals have been accelerated with the discovery of twist-bend nematic liquid crystals.[13,14] These materials, when doped with a chiral additive, form an oblique helicoidal phase at temperatures above the twist-bend phase transition. The heliconical pitch, and hence the reflection band of these materials can be tuned in E fields below 1 V μm^{-1}, so that the reflectivity shifts toward a shorter wavelength with increasing E.[15,16]

A more recent breakthrough was made possible after the discovery of the ferroelectric nematic liquid crystal (FNLC) phase.[17–22] This state exhibits macroscopic net electric dipole moment, (i.e., is spontaneously polarized) in zero external electric field, yet still possesses only orientational order. The spontaneous polarization, $\vec{P}$, (in all materials thus far reported) is parallel to the optic axis. This phase has drawn great interest over the past few years not only due to promising

M. S. H. Himel, A. Adaka, A. Jákli
Materials Sciences Graduate Program and Advanced Materials and Liquid Crystal Institute
Kent State University
Kent, OH 44242, USA
E-mail: ajakli@kent.edu

K. Perera, S. Sprunt, J. T. Gleeson, A. Jákli
Department of Physics
Kent State University
Kent, OH 44242, USA

P. Guragain, R. J. Twieg
Department of Chemistry and Biochemistry
Kent State University
Kent, OH 44242, USA

The ORCID identification number(s) for the author(s) of this article can be found under https://doi.org/10.1002/adfm.202413674

DOI: 10.1002/adfm.202413674

electro-optical properties[23,19] but also because FNLCs exhibit various instabilities,[24–26] form freestanding filaments,[27–29] and also show remarkable electromechanical responses.[30]

Recently also chiral ferroelectric nematic liquid crystals have drawn attention due to their[31–36] polar photonic properties. The director and accompanying polarization field in these materials spontaneously twist into a helical structure, $\vec{P}(z)$. Such polar helical structures were recently reported with two FNLC compounds: RM734[18] and DIO.[17] These were modified either by introducing a chiral center into the molecular structure[31,35] or using a chiral additive.[32,33] In contrast to the non-polar cholesteric phase, where due to the head-tail symmetry of the molecules the helical period corresponds to a π turn of the director, in the polar case the period doubles to a full 2π turn of the polarization field. However, the optical bandgap is still determined by a π rotation of the director, leading (as in nonpolar cholesterics) to selective reflection of normally incident light at wavelength $\lambda = \bar{n} \cdot p$.

Recently, it was found that the peak reflectivity of RM734 containing low concentrations of the chiral dopant BDH1281 can be reversibly tuned over $\Delta\lambda \approx 150$ nm by $E \leq 0.1\text{V}\,\mu\text{m}^{-1}$ applied perpendicular to the helical axis.[33] This shift toward the red, caused by an in-plane field, was explained as a rotation of the director at the substrates to compensate for the increase of twist elastic energy in the regions where the molecular orientation changes rapidly.[33] This result was confirmed by Ortega et al.[34] and agrees with previous observations by Nishikawa and Araoka.[32] In addition to the $\lambda = \bar{n} \cdot p$ reflection peak, which is observable at zero field, Ortega et al.[34] also observed m^{th} (1st and 3rd–6th) order optical bands under electric fields with $\lambda_m = \frac{2\bar{n}\cdot p}{m}$ peak wavelengths. Note, with this notation the zero field reflection wavelength $\lambda = \bar{n} \cdot p$ corresponds to second order band, $\lambda_2 = \frac{2\bar{n}\cdot p}{2}$. These results were quantitatively explained using Berreman's method,[34] revealing that chiral FNLCs are electrically tunable multiple band-gap photonic materials. These observations were made at temperatures well above ambient; this hampers their suitability for technological applications.

In this paper, we describe the electrical tuning of the reflectivity using mixtures that exhibit the FNLC phase at ambient temperature. We show that the tuning of the $\lambda_m = \frac{2\bar{n}\cdot p}{m}$ bands depend strongly on both the frequency of the sinusoidal applied field as well as on the mixture composition. Importantly, while in general, the reflectivity depends on the applied field, in some cases the broadband reflectivity can be tuned with no wavelength shift.

2. Experimental Section

Two mixtures that exhibit the FNLC phase at room temperature were used: KPA-02 and FNLC 919, and were selected as starting materials. KPA-02 was a mixture containing 60 wt.% of a newly synthesized, ferroelectric nematic liquid crystal compound, RT12155, and 40 wt.% of a commercially available nematic liquid crystal preparation, HTG-135200-100 (clearing point $T_c = 97$ °C) from HCCH. The molecular structure and synthetic route for RT12155, together with its calorimetry data are presented in the Supporting Information.

On cooling, KPA-02 has an isotropic to FNLC phase transition at 47 °C. The ferroelectric phase is stable below room

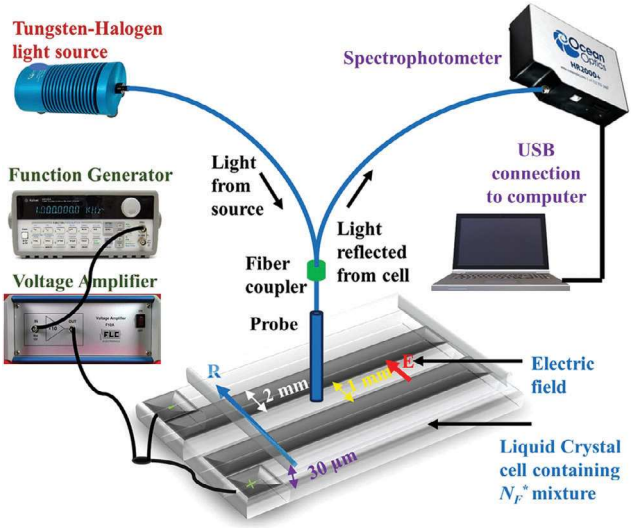

Figure 1. Schematic of the liquid crystal cell and the experimental setup for the electrically tunable reflectivity measurements of the room temperature ferroelectric nematic liquid crystal mixtures doped with chiral dopants. A combination of function generators and amplifiers was used to apply the voltages between in-plane Indium Tin Oxide (ITO) electrodes separated by $L = 1$ mm electrode gap. An OceanOptics HR2000+ spectrophotometer and a Tungsten-Halogen light source were used to measure the reflectivity. The reflection spectra have been collected by a computer connected to the spectrophotometer.

temperature. FNLC-919 has two nematic phases N_1 and N_2 above the N_F phase with the phase sequence I 80 °C N_1 44 °C N_2 32 °C N_F 8 °C Cr on cooling. The birefringence of FNLC 919 at room temperature was reported[37] to be $\Delta n \approx 0.22$ at 550 nm. The ferroelectric polarization of pure FNLC-919 is $0.047\frac{C}{m^2}$ at 25 °C.[30] The spontaneous polarization of KPA-02 was measured to be $0.044\frac{C}{m^2}$ at 33 °C (Figure S9, Supporting Information). To induce chirality, a commercially available chiral dopant, BDH1281 (molecular structure is shown in Figure S8, Supporting Information), having nominal helical twisting power $HTP \approx 100\,\mu\text{m}^{-1}$ was used. Three chiral mixtures of KPA-02 were studied with 3.2, 2.5, and 2 wt.% BDH1281 concentration, and one mixture of FNLC-919 with 2.5 wt.% BDH1281 concentration. All formulations exhibited wavelength-dependent reflectivity in the visible range. The pitches for the 3.2, 2.5, and 2 wt.% KPA 02+ BDH1281 blends were 0.29, 0.38, and 0.46 μm, respectively. The pitch for the 2.5 wt.% FNLC919 +BDH1281 blend was 0.37 μm.

Liquid crystal sandwich cells were prepared. These comprised two parallel glass plates to confine the LC; the plates were separated by $d \approx 30$ μm spacers. The surface of one plate has two electrically conducting strips (electrodes) that were parallel and separated by $L = 1$ mm gap. Since $d \ll L$, applying a potential difference between the electrodes yields an electric field almost entirely in the plane of the LC layer. An alignment layer (rubbed polyimide PI-2555) was deposited on both plates. The direction of rubbing was perpendicular to the electrodes (and hence parallel to the applied electric field). A schematic of the liquid crystal cell and the experimental setup for the optical measurements under various electric fields are shown in **Figure 1**.

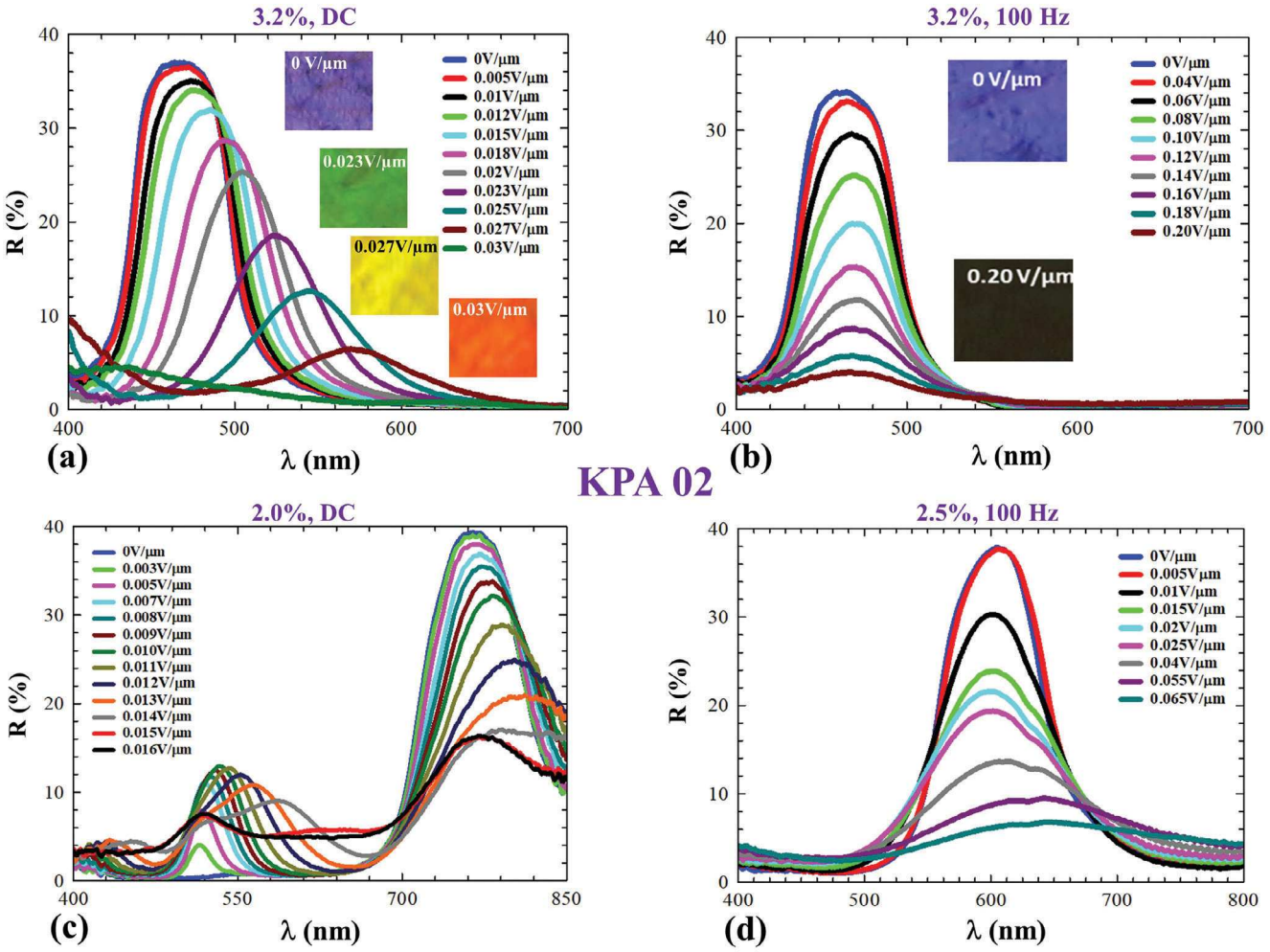

Figure 2. Electric field dependences of the reflection spectra of KPA-02 mixtures with 3.2%, 2.0%, and 2.5% BDH 1281chiral dopant concentrations. a) A mixture with 3.2% chiral dopant concentration under DC electric fields. Insets show microscopic textures in reflection at 4 different fields. b) The same mixture as in (a) under 100 Hz sinusoidal electric fields. Insets show microscopy textures in reflection at zero and 0.2 V/μm fields. c) A mixture with 2.0% chiral dopant under DC electric fields, showing 3 harmonics at each spectrum. d) A mixture with 2.5% chiral dopant under 100 Hz sinusoidal electric fields.

For applying the electric field, an HP 33120A function generator, and an FLC F20AD amplifier were used. All AC field values indicated below correspond to peak values (amplitude of the sinusoidal field). For the textural observations, the sample cells were placed in an Instec HS2000 heat stage and then viewed with an Olympus BX60 polarizing optical microscope. The reflectivity, $R(\lambda)$, was obtained using an OceanOptics VIS–IR spectrophotometer. The experimental protocol was to measure R as a function of the frequency and/or the amplitude of the potential difference.

3. Results

The electric field dependence of the reflection spectra (after subtracting the reflectivity of the empty cell) of KPA-02 mixtures with various chiral dopant concentrations is shown in **Figure 2**.

Figure 2a shows the spectra for a 3.2% chiral dopant concentration under DC electric field. At zero field the reflectivity maximum is 37% at 470 nm wavelength. The reflectivity decreases upon increasing DC field becoming only 6% at 0.027 V μm^{-1} field and immeasurable at 0.03 V μm^{-1}. In addition, the shape of the reflectivity curve evolves as the field increases; specifically, the reflectivity peak increases to 580 nm at 0.027 V μm^{-1}. This causes a change in the film's apparent color (under white illumination) as can be seen in microscope images (inset in Figure 2a) for 0, 0.023, 0.027, and 0.03 V μm^{-1} fields. This response is similar to that found by Feng et al.[33] in RM734 at elevated temperatures doped with the same chiral agent. Thus, the behavior at DC excitation agrees with published work.

For sinusoidal excitation, even at relatively low frequency, the results are notably different. Figure 2b shows the reflection spectra measured in the same mixture as in Figure 2a, but under 100 Hz sinusoidal electric fields. With 100 Hz AC field, and in contrast to the RM734 + 2% BDH1281 blends,[33] the peak positions are basically constant; it is only the overall reflectivity that decreases from 35% at zero field to ≈4% under 0.20 V μm^{-1}

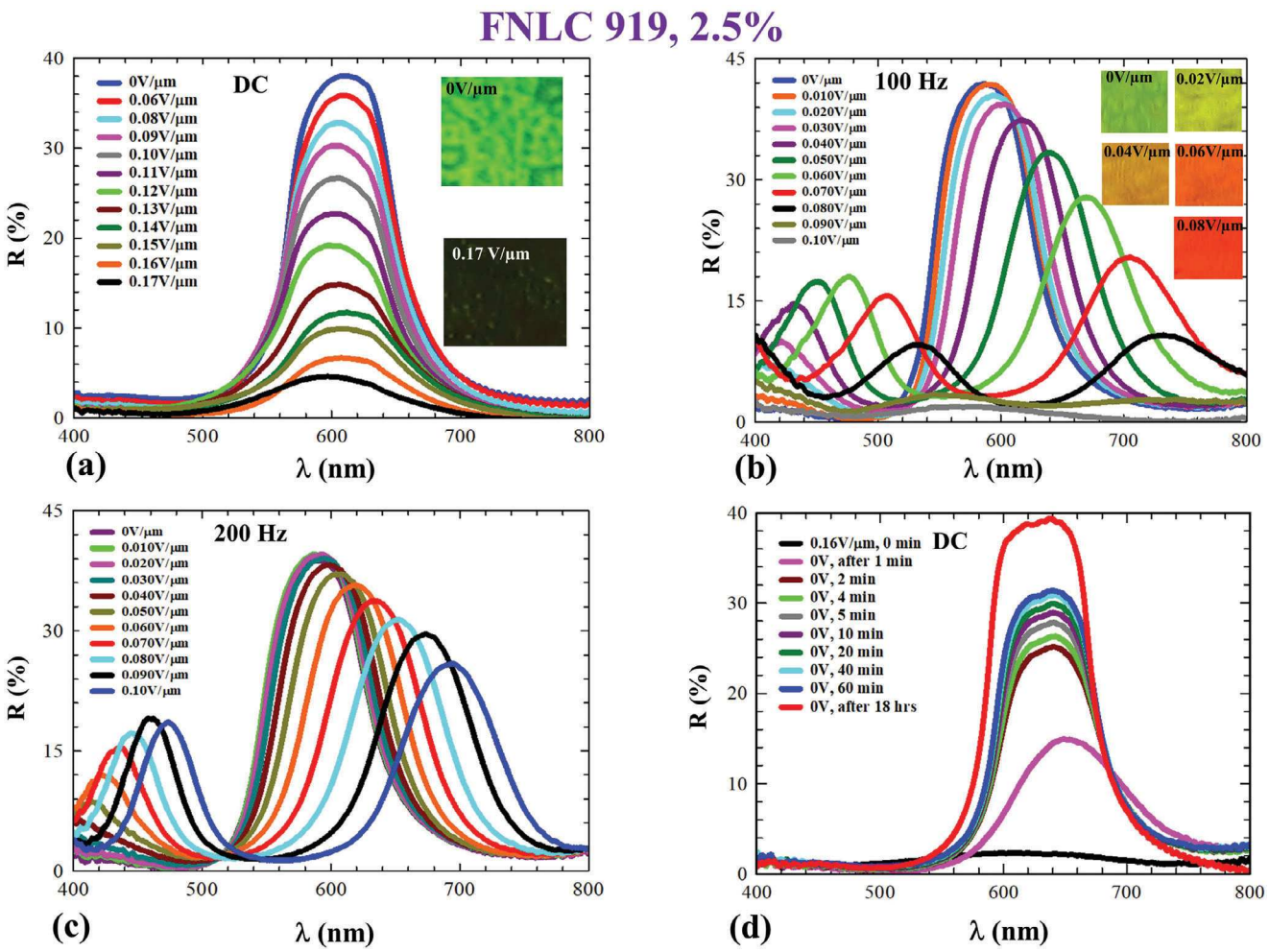

Figure 3. Wavelength and time dependences of the reflectivity for FNLC 919 NF mixture doped with 2.5% BDH 1281. a) Reflection spectra measured under 0 – 0.17 V µm^{-1} DC electric fields. Insets show microscopy pictures taken in reflection at 0 and 0.17 V/µm fields. b) Reflection spectra measured under 0 – 0.10 V µm^{-1} 100 Hz sinusoidal electric fields. Insets show microscopic pictures taken in reflection at 0 – 0.08 V µm^{-1} fields. c) Reflection spectra measured under 0 – 0.10 V µm^{-1} 200 Hz sinusoidal electric fields. d) Reflection spectra in 0–18 h time interval after 0.16 V µm^{-1} DC voltage was turned off at t = 0.

field (at the peak wavelength). The insets show that the reflection color changes from blue to black (corresponding to no reflection). Such an electrically-switchable reflectivity without color change can have various applications, but it is unexpected in view of the previous results obtained on high-temperature chiral FNLC materials[31–35] and will be discussed later.

In addition to the nature of the electric field, the dopant concentration (and thus presumably the helical pitch) also qualitatively affects the reflectivity. Figure 2c 2.0% chiral dopant in KPA-02 subject to DC electric fields. The strongest reflection peak ($\lambda_2 = \bar{n}p$) occurs at 750 nm. Additional peaks are observed at 1/3 and 1/4 of this value at $\lambda_3 \approx 490$ nm and $\lambda_4 \approx 420$ nm. For the KPA-02 / 3.2% BDH 1281 blend, these additional peaks would not be detectable with our present instrumentation. The amplitudes of these peaks increase with increasing field, as reported by Nishikawa and Araoka[32] and Ortega et al.[34] Figure 2d shows the reflection spectra of a film with 2.5% dopant concentration under a 100 Hz sinusoidal electric field. The difference in the wavelength of the maximum reflectivity shown in Figure 2b–d is in accordance with their pitch values p and the average refractive index ($\bar{n} \approx 1.6$) of the blends corresponding to $\lambda_2(3.2\%) \approx 290\ \text{nm} \times 1.6 \approx 464$ nm and $\lambda_2(2.5\%) \approx 380\ \text{nm} \times 1.6 \approx 608$ nm peak wavelengths. Similar to Figure 2b, the principal reflection wavelength only slightly varies with field. Similar to the cases in Figure 2a–c, the peak reflectivity decreases from ≈37% to less than 5% on increasing the field from $E = 0$ to 0.065 V µm^{-1}.

Figure 3 summarizes the reflectivity response of a 30 µm thick, planar aligned film composed of FNLC-919 doped with 2.5% BDH 1281. Figure 3a shows reflectivity measured subject to DC electric field varying from 0.00 to 0.17 V µm^{-1}. Similar to Figure 2b, the peak reflectivity is almost independent of the electric field. The reflection microscopy images at 0.00 and 0.17 V µm^{-1} fields are shown in the inset; these reveal how the layer switched between green-reflecting and non-reflecting states. Figure 3b shows reflectivity measured subject to electric fields varying from 0.00 to 0.17 V µm^{-1}, but at 100 Hz, sinusoidal oscillation. The behavior is similar to KPA-02 with both 3.2% and 2% dopant concentrations under DC fields. Insets show

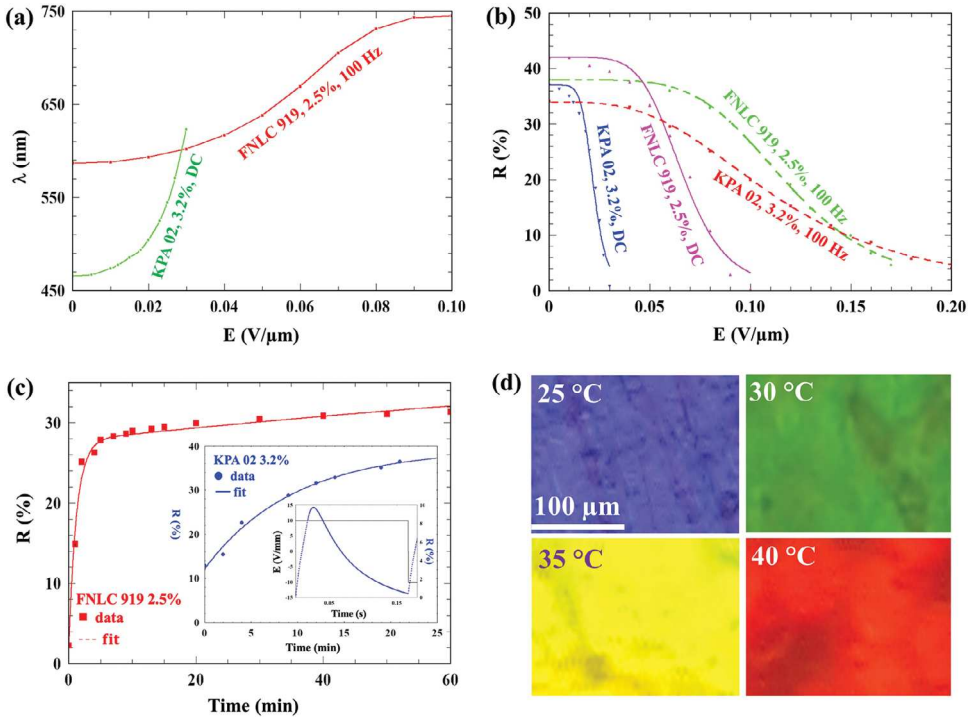

Figure 4. Electric and time dependences of the reflected wavelengths and reflectivities, and temperature dependences of the reflected colors of KPA-02 doped with 3.2% BDH 1281. a) DC and 100 Hz field dependences of the reflected wavelength for KPA-02 doped with 3.2% BDH 1281 and for FNLC 919 doped with 2.5% BDH 1281, respectively. b) Comparison of DC and 100 Hz AC electric field dependences of the reflectivity for KPA-02 doped with 3.2% BDH 1281, and for FNLC 919 doped with 2.5% BDH 1281. Data points were fitted by $R(E) = \frac{a\%}{1+b\cdot E^c}$ functions. Best fit parameters are a = 37, 42, 34 *and* 38; $b = 1.1 \cdot 10^{11}$, $1.3 \cdot 10^7$, 1041 and $3.7 \cdot 10^4$; c = 6.7, 6.0, 4.95 and 3.18 for 3.2% CD KPA-02, at DC; 2.5% CD FNLC 919 at DC; 3.2% CD KPA-02, at 100 Hz and 2.5% CD FNLC 919 at 100 Hz systems. c) Time dependence of the peak value of the reflectivity. Main pane: 2.5% CD FNLC 919 blend in 0 − 60 min time interval. Larger inset: 3.2% CD KPA-02 blend in 0 − 25 min time interval. Smaller inset: Time dependence of the reflectivity for the 3.2% CD KPA-02 blend under 3 Hz, 0.01 V/μm square wave field. d) Reflected colors of KPA-02 doped with 3.2% of BDH 1281 at 25, 30, 35, and 40 °C.

reflection microscopy images at 0 − 0.08 V μm^{-1} AC fields. The observed frequency dependence in chiral FNLC-919 samples contrasts sharply with that found in the doped KPA-02 samples, where the wavelength variation was absent under the AC field and present in DC fields. Figure 3c shows reflection spectra measured under 0–0.10 V μm^{-1} 200 Hz sinusoidal electric fields. Compared to the observations at 100 Hz, one can see that the wavelength tuning range decreased by ≈30 nm (≈25%), while the reflection tuning range decreased by ≈36%. Figure 3d shows the reflection spectra several times in the 0–18 h interval after 0.16 V μm^{-1} DC voltage was turned off.

The DC and 100 Hz field dependences of the reflectivity peak for KPA-02 with 3.2% dopant and for FNLC 919 with 2.5% dopant concentrations, respectively, are compared in **Figure** 4a. In both cases, at low fields the wavelength increases slowly; the increase becomes greater as fields exceed $E \approx$ 0.01 V μm^{-1} (DC) for the 3.2% doped KPA-02 and at $E \approx$ 0.05 V μm^{-1} (100 Hz AC) for the 2.5% doped FNLC 919. For the FNLC 919 mixture, the field dependence saturates above ≈ 0.08 V μm^{-1}, which is similar to the behavior observed for the chiral RM734 system.[33] In the KPA-02 mixture, the reflectivity drops sharply so that saturation is not observed. The DC and 100 Hz electric field dependences of the reflectivity for the 3.2% doped KPA-02, and the 2.5% doped FNLC 919, blends are shown in Figure 4b. At low fields, there is no change with the electric field, and then the reflectivity decreases rapidly, with the curve flattening when the reflectivity drops to ≈10%. This behavior could be fitted by an empirical function: $R(E) = \frac{a\%}{1+b\cdot E^c}$ with best fit parameters noted in the caption. The construction of the empirical R(E) is motivated by the notion that the reflectivity starts decreasing when the electric torque overcomes the elastic torque $\approx K(\frac{2\pi}{p})^2$ that corresponds to the constant in the denominator. The electric torque that comes mainly from the ferroelectric polarization, is represented by a $b \cdot E^c$ function. As the director is either parallel or perpendicular to the polarization, it is mainly governed by the director fluctuation. We note that the fit is relatively weak when the reflectivity starts to drop rapidly. This indicates that the parameter b itself has some field dependence.

While the reflectivity drops to almost zero within 1 *s* when the field is switched on to its corresponding maximum value, the relaxation to the original reflectivity values takes much longer time as shown in Figure 4c for 2.5% doped FNLC 919 blend 60 min after the field drops to zero. The decay is adequately described by a sum of two exponential decays, one fast and one slow: $R(t) = 25.5\%(1 - \exp(-t/\tau_{fast}) + 13.9\%(1 - \exp(-t/\tau_{slow}) + 2.22\%$, where we find $\tau_{fast} \approx 1$ min, $\tau_{slow} \approx 120$ min. Due to this longer relaxation process, it took ≈18 h for the original

reflectivity to recover fully. For the KPA-02 the reflectivity already increased to 10% within the first minute. From that point, the behavior is well-described with a single exponential R(t) = 27.0%(1 − exp(−t/τ_{slow})) + 10%,where $\tau_{slow} \approx 10$ min is 12 times smaller than observed in FNLC 919. Since a faster relaxation was not observed with this measurement protocol, we opted to find R using a low-frequency (3 Hz), 0.01 V μm^{-1} square wave. This behavior is shown in the smaller inset and shows that during the sign inversion (when the applied field goes over to zero field), the reflectivity increases to almost 10% indicating $\tau_{fast} \approx 30$ ms. We note that the percentages of the fast and slow decays were determined from the best fits where these percentages were fit parameters. The fast percentages determined from the best fits correspond well with the percentages where the slopes of the curves decrease considerably, indicating that the fits are reasonably good.

The colors reflected most strongly depend not only on the electric field but also on the FLC temperature. This is shown in Figure 4d, for the 3.2% doped KPA-02 mixture; the apparent color (with white illumination) changes from blue at 25 °C to red at 40 °C. Such behavior indicates increasing helical pitch on heating, which is opposite to the trend observed for the chiral RM734 system by Feng et al.[33]

4. Discussion

In this paper, we have studied two room temperature, chiral doped, ferroelectric nematic liquid crystal mixtures and demonstrated that the wavelength-dependent reflectivity, $R(\lambda)$, can be tuned by adjusting the amplitude and/or the frequency of an applied electric field, or the FNLC temperature. Interestingly, for KPA-02 using a DC field, both the overall reflectivity as well as its peak wavelength could be tuned simultaneously. In distinction, for FNLC 919 the peak wavelength does not change. On the other hand, at frequencies above 100 Hz, the peak wavelength is tunable for FNLC 919, but not for KPA-02. The tuning of the reflection color was previously demonstrated and explained,[33,34] however the electric field dependence of the reflection amplitude was noted and explained only for the $\lambda_1 = 2\bar{n} \cdot p$ and the $\lambda_3 = \frac{2\bar{n} \cdot p}{3}$ peaks.[32] Although Feng et al.[33] showed that the amplitude of the $\lambda_2 = \bar{n} \cdot p$ peak decreases while the peak location increases, they did not suggest a mechanism for this. Moreover, variation of the overall reflectivity without change in peak wavelength has not been previously reported. In the following, we propose a qualitative explanation of the field-induced tuning of the reflection amplitude and also attempt to explain why the two materials studied behave oppositely with DC versus AC applied field.

4.1. Reflectivity Tuning

The tuning of the reflection amplitude without changing the reflected color requires deformation of the zero-field helical polarization $P(z) = P_o cos(2\pi z/p_o)$ (see **Figure 5a** for $E = 0$). As the electric field along x increases, the fraction of polarization oriented in the $+x$ direction increases and the fraction in the $-x$ direction decreases without changing the periodicity. At increasing fields, this trends toward a periodic squared pulse function (see Figure 5a) for $E > 0$) described as $P(z) = \{_{-P} \; {}^{P} \quad {}^{|z| < l}_{l < |z| < p_o/2}$. The amplitudes a_m of the m^{th} Fourier peaks of such periodic structure become $a_m = \frac{1}{p_o} \int_0^l e^{-j2\pi z/p_o} dz = \frac{\sin(\frac{\pi m l}{p_o})}{m\pi}$. These amplitudes indeed decrease for decreasing $l < p_o/2$, in accordance with the observed decrease in the intensity of the selective reflection at increasing electric fields. This may explain the electric field-induced tuning of the reflection amplitude observed at 100 Hz for the chiral KPA-02 and at DC for chiral FNLC 919 blends.

The reflectivity tuning without change in peak wavelength happens in frequency-dependent fields where the azimuthal surface anchoring is stronger than the ferroelectric torque. Neglecting the dielectric torque, the torque due to the applied field is the ferroelectric torque $\Gamma_{FE} = P \cdot E \cdot \sin\varphi$, where φ is the angle between the polarization and the electric field. This is balanced by the twist elastic torque, $\Gamma_t = K_{22} \frac{d^2\varphi}{dz^2}$ and the viscous torque $\Gamma_v = -\gamma_1 \frac{d\varphi}{dt}$, where K_{22} is the twist elastic constant and γ_1 is the rotational viscosity, leading to the equation,

$$P \cdot E \cdot \sin\varphi + K_{22} \frac{d^2\varphi}{dz^2} - \gamma_1 \frac{d\varphi}{dt} = 0 \tag{1}$$

Equation (1) was analytically solved for deformed helix ferroelectric smectic liquid crystals,[38] for AC electric fields well below the unwinding field $E_u = \frac{K_{22}}{p_o^2 P}$, and the spatial dependence of φ was found to be

$$\varphi(z) = \frac{2\pi z}{p_o} + \frac{P E p_o^2}{4\pi^2 K_{22}\left(1 + \left(f/f_c\right)^2\right)} \left(\cos\left(2\pi f t\right) + f/f_c\right) \sin\left(2\pi f t\right)\sin\left(\frac{2\pi z}{p_o}\right) \tag{2}$$

where $f_c = \frac{2\pi K_{22}}{\gamma_1 p_o^2}$ is the critical frequency. According to Equation (2), at a constant electric field, the amplitude of the deformation (reflectivity) decreases as $\frac{P E p_o^2}{4K_{22}\pi^2(1+(f/f_c)^2)}$. This is comparable with the observed decrease of the variation of the reflectivity between DC and 100 Hz for KPA-02 (see Figure 2a,b) and between DC and 200 Hz (Figure 3a–c) for FNLC 919. Note, the critical frequency for $K_{22} \approx 3$ pN, $\gamma_1 \approx 1$ Pas and $p_o \approx 0.4$ μm, which are reasonable values for our studied materials, provide $f_c \approx 100$ Hz for the critical frequency, which is comparable with our observations.

After switching the field off, we found 2 timescales for the reflectivity to return to its original value: the majority of the reflectivity recovered quickly, while the remainder occurred on time scales two orders of magnitude longer. We attribute the fast relaxation to the relaxation of the twist deformation with a recovery time $\tau_{fast} \approx \frac{\gamma_1 p_o^2}{4\pi^2 K_{22}}$. For KPA-02 we found $\tau_{fast} \approx 30$ ms, which is ≈20 times smaller than what we observed for FNLC 919. As the pitches are similar, and assuming similar K_{22} values, this indicates a much higher rotational viscosity for FNLC 919 than for KPA-02. The slow relaxations are likely due to defect annihilations that are indicated by slow textural changes.

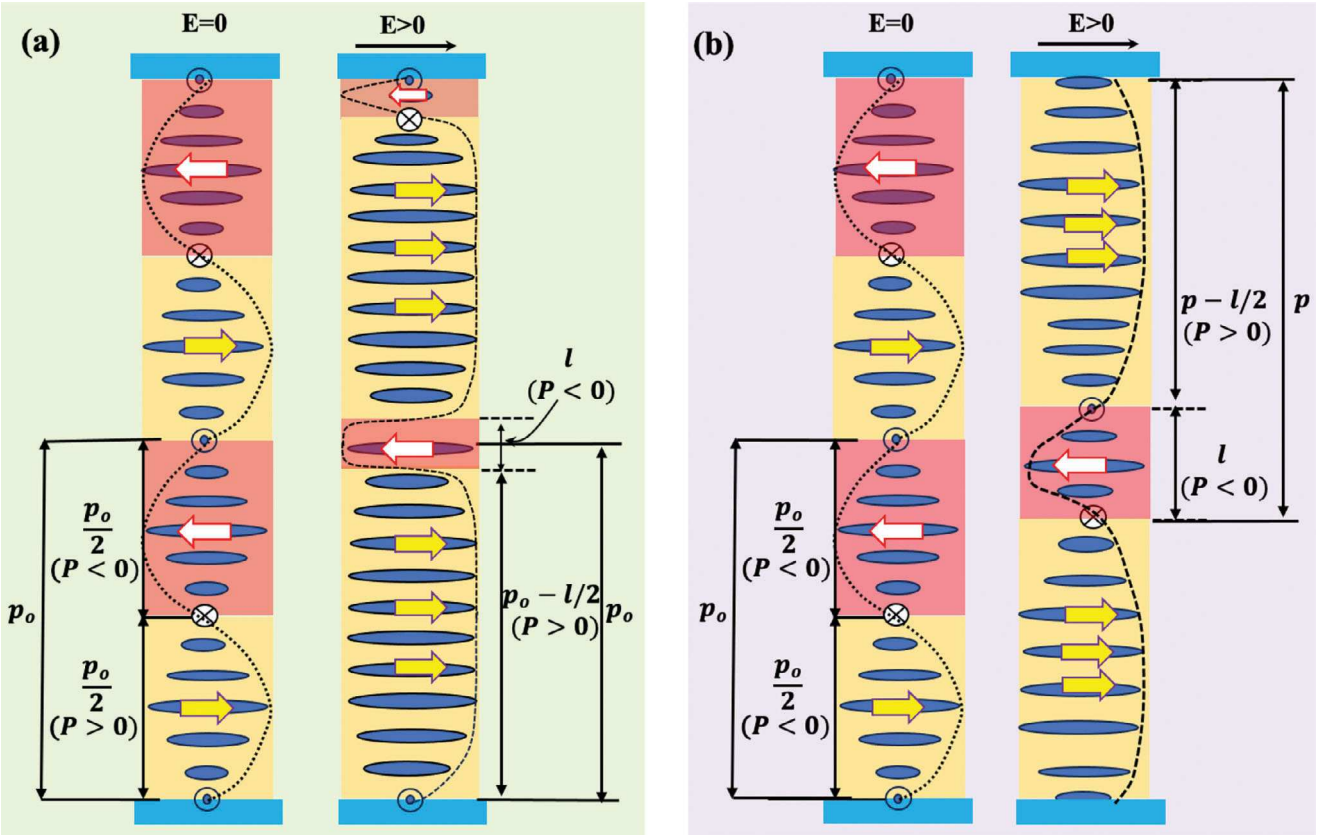

Figure 5. Illustration of the director and polarization field in in-plane electric fields. a) Qualitatively expected deformation when the azimuthal anchoring is assumed to be strong, leading only to the variation of the reflectance. b) Qualitatively expected deformation when the azimuthal anchoring is weak, leading to rotation of the director at the surface and causing the variation of the reflected wavelength, $\lambda_2 = \bar{n} \cdot p$.

4.2. Color Tuning

According to our observations, the shift of reflectivity peaks at $\lambda_2 = \bar{n} \cdot p$ is always accompanied by tuning of overall reflectivity. As proposed in prior work,[33] the λ_2 tuning requires azimuthal rotation of the director at the boundaries, as illustrated in Figure 5b for $E > 0$. Assuming the dielectric torque can be neglected with respect to the ferroelectric one, the director rotation on the surface occurs when the ferroelectric energy per unit area, $|\vec{P}| \cdot |\vec{E}| \cdot \xi$, where $\xi = \sqrt{\frac{K_{22}}{P \cdot E}}$ is the electric coherence distance, overcomes the azimuthal anchoring energy per unit area W_a. This torque competes the azimuthal anchoring energy per unit area W_a, leading to the equation for the threshold electric field for director rotation $\sqrt{K_{22} P E_{th}} = W_a$, giving that $E_{th} = \frac{W_a^2}{K_{22} P}$. With typical values $W_a \approx 3 \cdot 10^{-5} \frac{J}{m^2}$, $K_{22} \approx 3\ pN$ and $P \approx 4 \cdot 10^{-2}\ \mathrm{C\,m^{-2}}$, we get $E_{th} \approx 10^{-2}\ \mathrm{V\,\mu m^{-1}}$, which is comparable to the threshold for the λ_2-tuning observed for the KPA-02 under DC field (see Figure 4a) and a few times smaller than observed for the FNLC 919 at 100 Hz.

In contrast to the reflectivity tuning which does not require rotation of the director at the surfaces, the wavelength tuning does require it. The necessary conditions of the director rotation at the surfaces are: i) the ferroelectric torque should overcome the anchoring strength, and ii) the frequency of the AC field should be low enough. The second condition is governed by the surface viscosity: the lower it is, the higher the frequency where the wavelength tuning can be observed. For the KPA 02 at 100 Hz we already do not observe the wavelength tuning, while for the FNLC 919 we can observe it even at 200 Hz (although to at less extent than for 100 Hz). This indicates that the surface viscosity is larger for KPA 02. Considering the slightly stronger wavelength tunings of the 2.5% blend than of the 3.2% blend, we propose that the surface viscosity may slightly increase with the chiral dopant concentration.

While the observation that both the reflectivity and the reflection wavelength can be tuned with electric fields is characteristic of all studied materials and likely are general properties of chiral ferroelectric materials, the dynamics of the tuning seem to depend strongly on the individual material properties. The opposite behavior of the KPA 02 and FNLC 919 under DC field, i.e., large wavelength tuning of the KPA 02 blends and the lack of λ_2 shift for FNLC 919 at DC fields up to $E = 0.17\ \mathrm{V\,\mu m^{-1}}$ field (see Figure 3a) is our most surprising observation. We hypothesize that it might be related to the difference between the static and dynamic frictions that govern the rotation of the LC molecules at the surface under DC and AC fields. Perhaps the static friction for FNLC 919 is much larger than that of KPA 02, while the

dynamic surface viscosity of FNLC 919 is smaller than that of KPA 02.

To summarize, we have demonstrated how both overall reflectivity, as well as its peak wavelength, can be adjusted using two room temperature chiral, ferroelectric nematic liquid crystals. This can be accomplished by less than 0.2 V μm^{-1} external electric fields. While the peak wavelength shift is always accompanied by the variation of the overall reflectivity, under appropriate conditions the overall reflectivity could be reversibly varied between 0% and 40% without a shift in the peak wavelength. Electrically switchable reflection devices will be valuable in applications as varied as alternate reality/virtual reality applications to smart architectural windows. Lastly, we note that these devices can be made polarization-independent simply by stacking two devices that are identical except for having opposite handedness chirality.

Supporting Information

Supporting Information is available from the Wiley Online Library or from the author.

Acknowledgements

This work was supported by US National Science Foundation grant DMR-2210083. The material FNLC 919 was provided by Merck Electronics KGaA, Darmstadt, Germany.

Conflict of Interest

The authors declare no conflict of interest.

Data Availability Statement

The data that support the findings of this study are available from the corresponding author upon reasonable request.

Keywords

chirality, ferroelectric nematic liquid crystals, selective reflection color, switchable mirrors

Received: July 29, 2024
Revised: September 3, 2024
Published online:

[1] S. Nundy, A. Mesloub, B. M. Alsolami, A. Ghosh, *J. Clean Prod.* **2021**, *301*, 126854.
[2] C. M. Lampert, *Sol. Energy Mater. Sol. Cells* **2003**, *76*, 489.
[3] J. Xiong, E. L. Hsiang, Z. He, T. Zhan, S. T. Wu, *Light Sci. Appl.* **2021**, *10*, 216.
[4] P.-G. de Gennes, *Phys. Today* **1974**, *5*, 333.
[5] J. L. Fergason, *Appl. Opt.* **1968**, *7*, 1929.
[6] G. H. Brown, *Anal. Chem.* **1969**, *41*, 26A.
[7] R. B. Meyer, *Appl. Phys. Lett.* **1969**, *14*, 208.
[8] F. J. Kahn, *Phys. Rev. Lett.* **1970**, *24*, 209.
[9] S. P. Palto, M. I. Barnik, A. R. Geivandov, I. V. Kasyanova, V. S. Palto, *Phys. Rev. E* **2015**, *92*, 032502.
[10] H. Nemati, S. Liu, R. S. Zola, V. P. Tondiglia, K. M. Lee, T. White, T. Bunning, D. K. Yang, *Soft Matter* **2015**, *11*, 1208.
[11] M. E. Mcconney, V. P. Tondiglia, L. V. Natarajan, K. M. Lee, T. J. White, T. J. Bunning, *Adv. Opt. Mater.* **2013**, *1*, 417.
[12] S. S. Choi, S. M. Morris, W. T. S. Huck, H. J. Coles, *Adv. Mater.* **2010**, *22*, 53.
[13] V. Borshch, Y.-K. Kim, J. Xiang, M. Gao, A. Jákli, V. P. Panov, J. K. Vij, C. T. Imrie, M. G. Tamba, G. H. Mehl, O. D. Lavrentovich, *Nat. Commun.* **2013**, *4*, 2635.
[14] D. Chen, J. H. Porada, J. B. Hooper, A. Klittnick, Y. Shen, M. R. Tuchband, E. Korblova, D. Bedrov, D. M. Walba, M. A. Glaser, J. E. Maclennan, N. A. Clark, *Proc. Natl. Acad. Sci.* **2013**, *110*, 15931.
[15] J. Xiang, S. V. Shiyanovskii, C. Imrie, O. D. Lavrentovich, *Phys. Rev. Lett.* **2014**, *112*, 217801.
[16] J. Xiang, Y. Li, Q. Li, D. A. Paterson, J. M. D. Storey, C. T. Imrie, O. D. Lavrentovich, *Adv. Mater.* **2015**, *27*, 3014.
[17] H. Nishikawa, K. Shiroshita, H. Higuchi, Y. Okumura, Y. Haseba, S. I. Yamamoto, K. Sago, H. Kikuchi, *Adv. Mater.* **2017**, *29*, 1702354.
[18] R. J. Mandle, S. J. Cowling, J. W. Goodby, *Phys. Chem. Chem. Phys.* **2017**, *19*, 11429.
[19] X. Chen, E. Korblova, D. Dong, X. Wei, R. Shao, L. Radzihovsky, M. A. Glaser, J. E. Maclennan, D. Bedrov, D. M. Walba, N. A. Clark, *Proc Natl. Acad. Sci.* **2020**, *117*, 14021.
[20] N. Sebastián, L. Cmok, R. J. Mandle, M. R. De La Fuente, I. Drevenšek Olenik, M. Čopič, A. Mertelj, *Phys. Rev. Lett.* **2020**, *124*, 037801.
[21] N. Sebastián, M. Čopič, A. Mertelj, *Phys. Rev. E* **2022**, *106*, 021001.
[22] R. Saha, P. Nepal, C. Feng, M. S. Hossain, M. Fukuto, R. Li, J. T. Gleeson, S. Sprunt, R. J. Twieg, A. Jákli, *Liq. Cryst.* **2022**, *49*, 1784.
[23] N. Sebastián, R. J. Mandle, A. Petelin, A. Eremin, A. Mertelj, *Liq. Cryst.* **2021**, *48*, 2055.
[24] R. Barboza, S. Marni, F. Ciciulla, F. A. Mir, G. Nava, F. Caimi, A. Zaltron, N. A. Clark, T. Bellini, L. Lucchetti, *PNAS* **2022**, *119*, 2207858119.
[25] M. T. Máthé, Á. Buka, A. Jákli, P. Salamon, *Phys. Rev. E* **2022**, *105*, L052701.
[26] M. T. Máthé, B. Farkas, L. Péter, Á. Buka, A. Jákli, P. Salamon, *Sci. Rep.* **2023**, *13*, 6981.
[27] M. T. Máthé, K. Perera, Á. Buka, P. Salamon, A. Jákli, *Adv. Sci.* **2023**, *11*, 202305950.
[28] S. Nishimura, S. Masuyama, G. Shimizu, C. Chen, T. Ichibayashi, J. Watanabe, *Adv. Phys. Res.* **2022**, *1*, 2200017.
[29] A. I. Jarosik, H. Nádasi, M. I. Schwidder, A. I. Manabe, M. I. Bremer, M. I. Klasen-Memmer, A. Eremin, *PNAS* **2024**, *121*, 2313629121.
[30] M. T. Máthé, M. S. H. Himel, A. Adaka, J. T. Gleeson, S. Sprunt, P. Salamon, A. Jákli, *Adv. Funct. Mater.* **2024**, *34*, 2314158.
[31] X. Zhao, J. Zhou, J. Li, J. Kougo, Z. Wan, M. Huang, S. Aya, *Proc. Natl. Acad. Sci.* **2021**, *118*, 2111101118.
[32] H. Nishikawa, F. Araoka, *Adv. Mater.* **2021**, *33*, 2101305.
[33] C. Feng, R. Saha, E. Korblova, D. Walba, S. N. Sprunt, A. Jákli, *Adv. Opt. Mater.* **2021**, *9*, 2101230.
[34] J. Ortega, C. L. Folcia, J. Etxebarria, T. Sierra, *Liq. Cryst.* **2022**, *49*, 2128.
[35] D. Pociecha, R. Walker, E. Cruickshank, J. Szydlowska, P. Rybak, A. Makal, J. Matraszek, J. M. Wolska, J. M. D. Storey, C. T. Imrie, E. Gorecka, *J. Mol. Liq.* **2022**, *361*, 119532.
[36] C. L. Folcia, J. Ortega, T. Sierra, A. Martínez-Bueno, J. Etxebarria, *Giant* **2024**, *19*, 100316.
[37] J. S. Yu, J. H. Lee, J. Y. Lee, J. H. Kim, *Soft Matter* **2023**, *19*, 2446.
[38] L. A. Beresnev, V. G. Chigrinovs, D. I. Dergachev, E. P. Poshidaev, J. Fünfschilling, M. Schadt, *Liq. Cryst.* **1989**, *5*, 1171.